Journal of Structural Geology 32 (2010) 997–1008

Contents lists available at ScienceDirect

Journal of Structural Geology

journal homepage: www.elsevier.com/locate/jsg

Drawing parallels: Modelling geological phenomena using constraint satisfaction

R. Edmunds*, B.J. Hicks, G. Mullineux

Innovative Design and Manufacturing Research Centre, Department of Mechanical Engineering, University of Bath, Bath BA2 7AY, UK

ARTICLE INFO

Article history:
Received 10 December 2009
Received in revised form
31 May 2010
Accepted 16 June 2010
Available online 30 June 2010

Keywords:
Parallel folding
Kink banding
Friction
Energy methods
Constraints
Optimization

ABSTRACT

This paper gives insight into the transition between the different folding-types seen in nature. Using constraint satisfaction and optimization to study least energy solutions of an elastic, frictional model for concentric parallel folding, kink band waveshapes resulting from the same model are discovered. Simplifying the concentric parallel folding model down to a two layer formulation, and assuming the geometry of the whole layered material is governed by this, the behaviour of the central interface is represented using a number of points whose displacement is constrained. With a linear foundation, the full large-deflection energy formulation reaches a point where the whole system is locked up after only two folds, matching experimental evidence. This is overcome by adding a nonlinearity to the foundation, where the sequential destabilization and restabilization of experimental load-deflection plots is observed and the wave-profiles agree with the naturally occurring geological phenomenon. Increasing the nonlinearity in the foundation and the magnitude of the overburden pressure, the phenomenology of the concentric folding model can be altered to one that is more kink band-like in structure. Thus a "trigger" is found, relating two prevalent folding patterns which are generally considered to be at opposite ends of the spectrum of geometries.

1. Introduction

This paper builds upon previous work (Hunt et al., 2006), which presented a rigorous analysis of serial concentric parallel folding. Fig. 1 shows a series of folds, where each fold has been instigated in sequence. Such behaviour is called serial (Blay et al., 1977), sequential (Peletier, 2001) or cellular (Hunt et al., 2000a; Hunt, 2006) buckling. Whilst many types of folds are observed in the field, the exact ordering or formation of the buckles is often not apparent. The process of serial folding has long been recognized by geologists as the most common phenomenon in the folding of rocks, with field observations (Price, 1970, 1975) and analogue experiments (Cobbold, 1975; Blay et al., 1977) supporting this. However, this type of behaviour is markedly different to the synchronous wave-trains—where all of the folds occur uniformly throughout the material—that are predicted by Biot's viscous models (Biot, 1961, 1963, 1964). In particular the wavelength resulting from sequential buckling does not correspond to the dominant wavelength, the one that amplifies most rapidly in the spontaneous formulation (Budd et al., 2001).

With folding occurring at many different levels of the Earth's crust, the rheology of the rocks during the folding process is often unknown. However, fold amplification is achieved by non-elastic (e.g. viscous or plastic) behaviour. In order to explore these processes, researchers have investigated a variety of theoretical approaches to aid the understanding of the phenomenology and the governing mechanisms. In particular, sophisticated analytic and numerical models have evolved as a result of the studies of both single and multilayer buckling of various rheological combinations by Biot and Ramberg (Biot, 1965; Ramberg, 1961; Ramberg and Strömgård, 1971).

Whilst Biot and Ramberg both recognized that elastic effects are important in the early stages of the folding process, they put the viscous effects as the dominant deformation type controlling the folding process. Opposing this idea, Johnson explored elastic-plastic deformation further, proving that behaviour similar to that observed in the Biot and Ramberg models could also develop in these models, although again only for synchronous folding (Johnson, 1977). This paper is complementary to these works, as it studies non-synchronous folds and shows that elastic buckling is of geological importance. Parallel folds in particular are usually found in the younger, upper parts of an orogenic belt which supports the use of elastic theory (de Sitter, 1964).

When an elastic multilayer comprising stiff material, embedded in a soft matrix, is loaded axially, the layers slip at the interfaces (Donath and Parker, 1964) and deform into the softer surrounding medium. The multilayer bends about the centres of curvature such that a regular periodic concentric buckle pattern is created (Fig. 1).

* Corresponding author. Tel.: +44 (0) 1225 385937.
E-mail addresses: R.Edmunds@bath.ac.uk (R. Edmunds), B.J.Hicks@bath.ac.uk (B.J. Hicks), G.Mullineux@bath.ac.uk (G. Mullineux).

0191-8141/$ – see front matter © 2010 Elsevier Ltd. All rights reserved.
doi:10.1016/j.jsg.2010.06.005

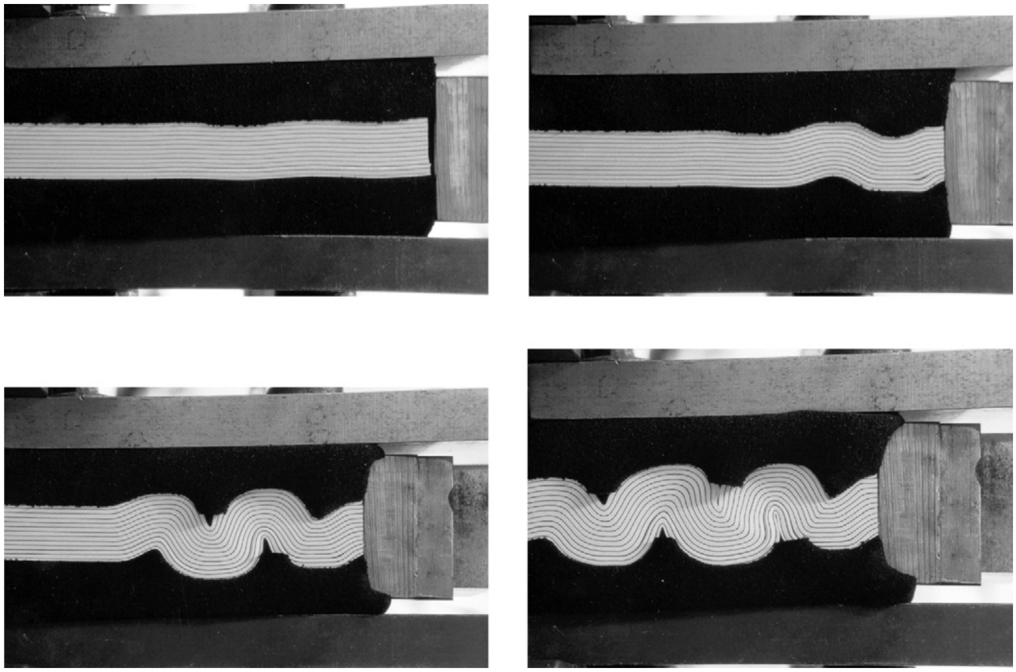

Fig. 1. Concentric parallel folding in layers of paper, showing the serial buckling behaviour.

Correspondingly, when the multilayer and foundation are of a similar competency and subjected to loading along the length, the layers are unable to move into the matrix and sections of the layers rotate across the width of the multilayer, forming straight limbs and sharp corners. This leads to *kink banding* or *box folding* (Price and Cosgrove, 1990) (Fig. 2).

As both concentric folding and kink banding phenomena only occur under high overburden pressure (Hobbs et al., 1976), the importance of the layering becomes paramount as the interfaces provide the natural slip planes necessary for the system to adopt these modes (Hobbs et al., 1976; Price and Cosgrove, 1990). Central to understanding this behaviour is the need to consider the frictional properties along the interfacial planes. These considerations have led to a series of papers that investigated multilayer slippage under large overburden pressures using elastic, frictional models. The formation of individual kink bands was initially considered by Wadee et al. (2004) and the propagation of this system to a series of bands was explored by Wadee and Edmunds (2005). The model was also extended to investigate fibrous materials (Edmunds and Wadee, 2005).

Limiting themselves to two layers and the formation of the initial buckle, Budd et al. (2003), assuming that the folding seen in nature corresponds to a minimal energy solution which penalizes voids, formulated a potential energy model for concentric parallel folding where deformation is by flexural buckling. This formulation includes an energy contribution due to the slip at the layer interface. By extending the model to a multilayer of n layers, Edmunds et al. (2006) were able to successfully compare the solutions of the formulation to the first instability of a set of experiments using layers of paper in foam. Using the small-deflection two layer formulation, a primitive form of serial buckling—following the transition from a single fold to a second fold (it was computationally too intensive to go beyond two folds)—was shown by Hunt et al. (2006), who restricted the waveshapes to cubic B-splines and added a restabilizing nonlinear component to the foundation. Of course, this imposed the waveshape upon the solution, rather than allowing a natural one to emerge from the formulation.

The shortcomings of using B-splines in this way are covered in a recent paper (Edmunds et al., submitted for publication), which uses constraint-based techniques to successfully follow the load–deflection paths and fold evolution of the small-deflection energy formulation over a number of humps. However, an additional consideration of the B-spline analysis is that it is difficult to apply the methodology to the full, large-deflection problem. The purpose of this paper is therefore to deal with explicitly the large-deflection formulation and the limitations of the B-spline approach.

Constraint-based modelling is concerned with *what* is to be achieved rather than *how* it is to be achieved. It is particularly useful in the early stages of problem solving where precise information is not available. Often in these stages exact knowledge of the solution is not possible, but rather a sense of the limitations placed upon the system is more apparent. The intersection of the limitations is then the feasible solution space. It is possible to explore the solution alternatives by creating a set of criteria that must be satisfied by the system—i.e. the *constraints*—finding a configuration that gives the smallest perturbation from these goals. To resolve the constraint set and thus find these configurations, a constraint-based modelling

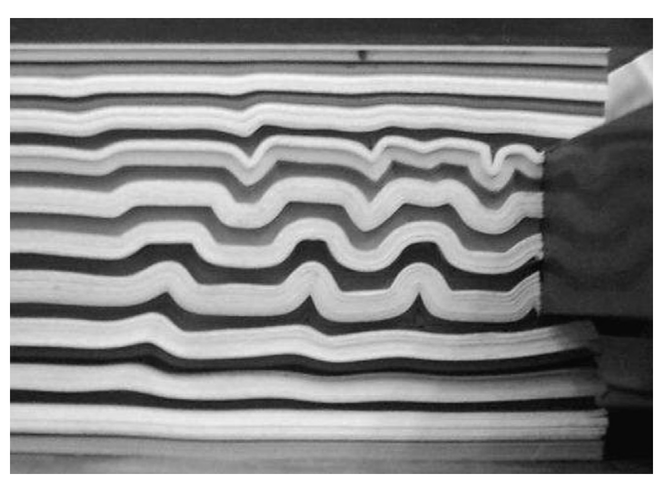

Fig. 2. Kink bands in paper.

environment (Mullineux, 2001) has been created which uses a number of optimization codes.

This methodology has been used effectively for many of the general engineering design applications that are found in practice, including products, machines and technical systems (Hicks et al., 2006; Mullineux et al., 2005). The constraint-based modeller in particular has been used to explore several engineering domains:

- Design synthesis and analysis of mechanisms (Mullineux et al., submitted for publication);
- Design analysis and optimization of machines (Hicks et al., 2001);
- Investigation of machine-material and machine–product interaction (Mullineux et al., in press);
- Evaluation of processing equipment to handle product variation (Matthews et al., 2006);
- Modelling and understanding of human motion (Mitchell et al., 2007).

The potential of a constraint-based formulation for modelling geological systems was identified by Edmunds et al., (submitted for publication) where it was applied to the developed concentric parallel folding formulation. It was shown that a constraint-based model gives good qualitative results, thus highlighting the ability of the formulation to model real geological folding.

In this paper, the constraint-based representation of the small-deflection energy model given by Edmunds et al. (submitted for publication) is extended to the full, large-deflection energy functional developed by Budd et al. (2003). To this end, the evolution of the central interface between two initially flat layers is explored by increasing the end-shortening and attempting to satisfy the constraints. This large-deflection problem could not be studied using B-splines. Additionally, it has long been of interest to investigate the parameter space such that other fold-profiles might be determined, this is easily done using constraints.

A summary of the two-layer potential energy formulation for concentric parallel folding presented in by Budd et al. (2003) is given in Section 2 as well as results from two subsequent follow-up articles (Edmunds et al., 2006; Hunt et al., 2006). In Section 3, the constraint-based methodology is briefly explained and the constraint-based modelling environment is introduced, along with a short discussion as to how this is applied to the problem presented here. For the large-deflection formulation, with both a linear and nonlinear foundation, output solution profiles and load–deflection plots are shown in Section 4. When the results are compared to experimental data obtained by Edmunds et al. (2006) and Boon et al. (in press), there is close phenomenological correspondence. Thus the simulations provide several interesting insights as to the processes that control the formation of a number of concentric folds. By altering certain parameters, the same formulation is extended to admit kink bands as a solution profile in Section 5—giving some elucidation into the natural phenomenology governing the transition between several prominent folding types. Finally conclusions are drawn.

2. Concentric parallel folding—nonlinear elastic, frictional model

Fig. 3 shows the load–deflection plot from a concentric parallel folding experiment using a multilayer of paper surrounded by a foam matrix and the destabilizing–restabilizating behaviour seen in this plot corresponds closely to the propagation of folds along the length of the sample seen in Fig. 1.

A brief explanation of the loading behaviour seen in Fig. 3 follows. Firstly the overburden pressure is applied transversely

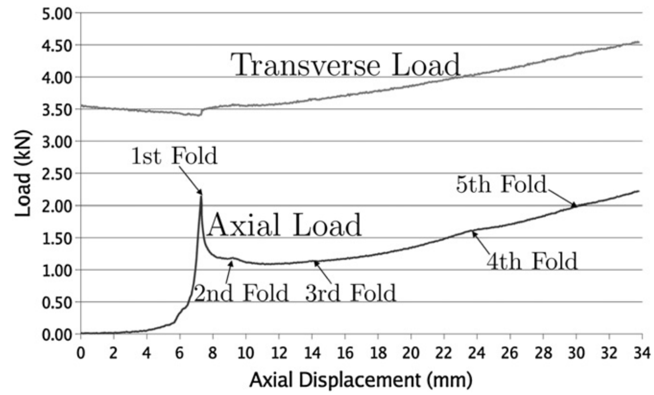

Fig. 3. Load–End-shortening plot from buckling experiments on multilayers of paper. (After Edmunds et al., 2006).

across the sandwich of layers and foam and is held at this level. After this an axial displacement is applied at a slow, constant speed and initially little happens as the system takes up the load (0–6 mm). As the layers are approximately flat, the in-line stiffness is large and the axial load begins to increase linearly (6–7 mm) until an instability occurs as the first fold forms and the systems softens. As the amplitude of the fold increases the load drops smoothly, before increasing slightly as some lock-up criterion is reached (7–9.5 mm). The second fold forms in a similar fashion, although the load drops to a much smaller extent (9.5–14 mm). The serial evolution of the folds thus continues in this manner—stiffening followed by instability in sequence (14–34 mm). In addition there is an overall restabilization of the axial load, which seems linked to the overburden. Once the initial instability has occurred, due to the application of the axial displacement, the overburden pressure rises as the sample opens up and some of the axial load is directed into the foundation. As is shown in Section 2.1 this change in the frictional properties results in a growth in axial load.

The purpose of this paper is to follow phenomenologically the cellular loading behaviour of the experiments such as that of Fig. 3, matching the destabilizing–restabilizing load–deflection path *after the initial instability* and by studying the output wave-profiles the propagation of the folds along the multilayer (Fig. 1). From energy considerations, Budd et al. (2003) simplified the system to just two layers and started to model this process for the initial instability; a primitive form of the evolution from a single fold to two folds (Fig. 4) was achieved by Hunt et al. (2006) by inserting two interacting cubic B-splines into the formulation, with a nonlinearity in the foundation, quantitatively following the early stages of Fig. 1. It is this same energy formulation that is extended in the formation of a constraint-based model.

2.1. Pseudo potential energy

In the first instance Budd et al. (2003) found a potential energy formulation for a simple two-layer model. This model was eventually extended to a multilayer of n layers by Edmunds et al. (2006).

Following Budd et al. two axially and transversely incompressible layers of thickness t are considered, formed from material with bending stiffness EI and embedded in a softer foundation material with transverse linear stiffness k per unit length. When compressed longitudinally by a load P, to fit without voids the layers must bend about the same centre of curvature. With the centrelines of the layers unchanged in length, differential stretching then generates slip at the interface between the layers (Fig. 5). The total potential energy, V, therefore includes a quasi-energy contribution due to the work done against friction during slip (U_μ). This is added to the

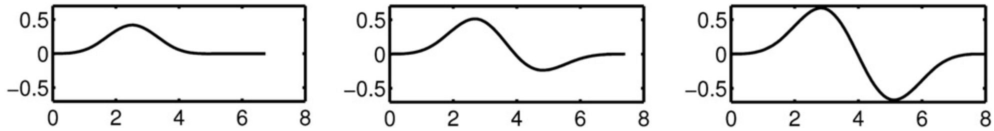

Fig. 4. Using B-splines to follow wave-profile evolution. (After Hunt et al., 2006).

other energy contributions: the bending energy (U_B) minus the work ($P\mathcal{E}$) done by the load (Thompson and Hunt, 1973)—$\mathcal{E}$ here is the end-shortening—plus the contribution from the foundation (U_{F_k}) (Hunt et al., 1993). The total potential energy function, V, valid over *large deflections* $w = w(x)$ is hence given by (Budd et al., 2003):

$$\begin{aligned} V &= U_B - P\mathcal{E} + U_{F_k} + \chi U_\mu \\ &= EI\int_0^L \left(\frac{\ddot{w}^2}{1-\dot{w}^2}\right)\mathrm{d}x - P\int_0^L \left(1-\sqrt{1-\dot{w}^2}\right) + \frac{1}{2}k\int_0^L w^2\mathrm{d}x\mathrm{d}x \\ &\quad + \chi\mu q t\int_0^L |\sin^{-1}\dot{w}|\mathrm{d}x. \end{aligned} \tag{1}$$

Dots denote differentiation with respect to the arclength x, and L is the length of the layers over which deformation takes place. μ and q are the coefficient of friction and overburden pressure respectively. The *friction indicator* $\chi = \pm 1$ indicates whether the friction term is positive or negative—depending on whether the friction acts to resist the release of strain energy or in the opposite sense.

If w is small then (1) reduces to

$$V = \int_0^L \left(EI\ddot{w}^2 - P\frac{\dot{w}^2}{2} + k\frac{w^2}{2} + \chi\mu q t|\dot{w}|\right)\mathrm{d}x. \tag{2}$$

The equilibrium solutions of the system on the verge of slipping are then stationary points of the energy functional $V(\mathcal{E}, L)$ as P varies and to see the form of these solutions Budd et al. (2003) limited the profile of the fold using a Galerkin approximation to give a sinusoidal waveshape. Putting this into (2), the resulting bifurcation diagram (Fig. 6(a)), which plots the stationary points, opens the bifurcation point at the classical Euler *critical load*, $P = P^C$ when $\mathcal{E} = 0$ (Thompson and Hunt, 1973). Thus the coefficient of friction, μ, and the friction indicator, χ, act as an imperfection. (Note that the paths at $\chi = +1$ are unstable under dead loading, but are stable when the end-shortening is controlled as in the experiments).

Using a single cubic B-spline, in place of the Galerkin approximation, Hunt et al. (2006) find a similar behaviour to that exhibited in Fig. 6(a). However, they also try to model the foundation in a more realistic manner by adding a nonlinear term to the foundation energy of the form:

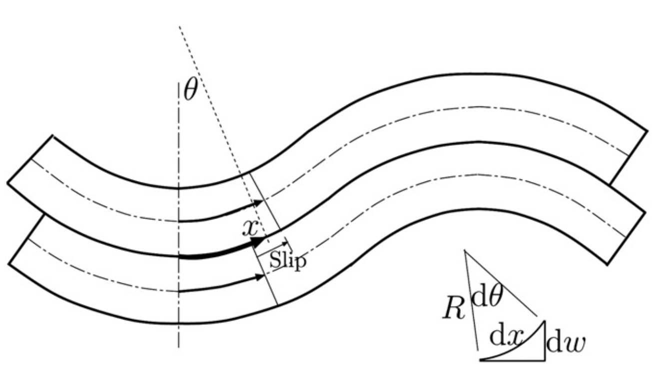

Fig. 5. Slip between incompressible layers constrained to remain in contact.

$$U_{F_C} = \frac{1}{4}C\int_0^L w^4\mathrm{d}x, \tag{3}$$

where C is a transverse stiffening nonlinearity. This is equivalent to the matrix exhibiting nonlinear elastic behaviour, where U_{F_k} and U_{F_C} represent a loss of stiffness, as the foundation buckles elastically, and a re-stiffening, as voids within the foundation are compressed (Hunt and Wadee, 1998). Thus, adding the nonlinearity (3) to (2), the system can restabilize and eventually lock-up at some larger value of $\mathcal{E}$ (Fig. 6(b)).

Looking at Fig. 6(a) in more detail, at constant load P, points in the region between the $\mathcal{E} = 0$ axis and the curve defined by $\chi = -1$ (or $\chi = +1$) are stationary positions where the system is "jammed" between two critical slip conditions which correspond to a half-wave with positive or negative amplitude and the friction opposing this motion. Within the jammed region the system sits in equilibrium; however, when placed outside of this, with constant load, it would return to the boundary. Thus at zero load, with sufficient end-shortening, the system stays at the $\chi = -1$ line. With increased load the system follows the dashed line on Fig. 6(a) through the jammed region, until at $\chi = +1$ it deflects with $\mathcal{E}$ increasing.

With a purely linear foundation, the critical load, $P = P^C$, can be calculated. Using the Galerkin approximation—a similar equation is found when a cubic B-spline is imposed as the waveshape—in (2) yields

$$P^C = \frac{2EI\pi^2}{L^2} + \frac{kL^2}{\pi^2}. \tag{4}$$

This is obtained by minimizing P^C over all values of L and P^C and occurs when

$$L = \pi\sqrt[4]{\frac{2EI}{k}}. \tag{5}$$

However, the length, L, is that associated with a wave-train; for serial buckling folds are likely to have arclengths different to that predicted by (5) (Budd et al., 2001).

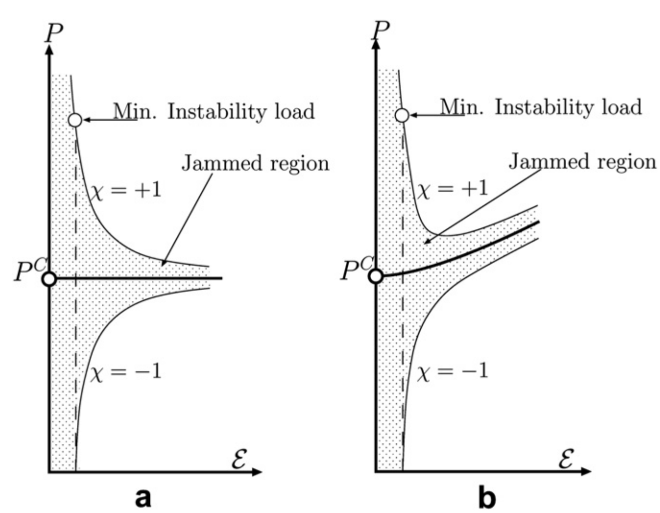

Fig. 6. Bifurcation diagram indicating jammed region for constant μ, for (a) A linear foundation, (b) A nonlinear foundation.

3. Constraint modelling

Whilst giving some initial insight into serial buckling, the cubic B-spline approximation (Hunt et al., 2006) using the small-deflection energy formulation is very computationally intensive for even the primitive two-fold case. It was not feasible to extend the model beyond two folds to a full sequence of folds. It was also not possible to study the large-deflection model.

Using the constraint-based methodology to formulate the problem, Edmunds et al. (submitted for publication) have shown that it is possible to explore the multi-fold solutions arising from the small-deflection formulation and achieve behaviour that can be effectively compared to the propagation observed during experiments. Here the latter problem is addressed: creating a constraint-based model of the full energy functional and studying the solutions arising from resolving the constraints.

A summary of the constraint-based methodology and its application to the elastic, frictional concentric parallel folding model follows.

3.1. Constraint-based techniques

Constraints on a process or system might be: geometric limitations, performance and physical requirements, limits on resources or more complex engineering considerations. Constraint-based reasoning uses these limitations as the core of the modelling process, representing them as a set of *constraint rules*, objectives that are required to be satisfied and are written algebraically as equality and inequality relations in a number of variables. To satisfy the constraints and hence find a valid solution, a configuration of the variables can be discovered where the *falseness* of the rules is minimized. Usually the constraints are not independent and so must be solved simultaneously; the solution space is the intersection of the spaces for each constraint.

There are several advantages in using a constraint-based methodology to model systems. However, resolving the imposed constraints can still be a problem and a variety of numerical and symbolic ways for resolving constraints currently exist (Mullineux, 2001). The constraint-based modelling environment (Mullineux, 2001) used in this work has a class of functions to define and resolve constraint rules. Fig. 7

Each constraint is put into a rule() command. A single objective function F is formed by evaluating the expression within each rule() statement and taking the sum of the squares of these. If $F = 0$, then each constraint is "true" and a feasible solution exists, otherwise its value is a measure of falseness. In this case the resolution process commences, varying a set of parameters specified by the user, in order to minimize F. If a (local) non-zero minimum is found, this suggests some constraints are in conflict, and the solution is a "best compromise".

Constraint resolution is performed using in-built *optimization routines*. Optimization techniques provide a viable means for resolving constraints as the number of variables and constraints are not limited and the constraints are not required to be in any particular form. For the problem described in this paper, it has been found that the NAG optimization routine, *e04wdc: nag_opt_nlp_solve*, (NAG, 2005) is the most appropriate for exploring the solution space.

Designed to solve nonlinear programming problems—the minimization of a smooth nonlinear function subject to a set of constraints on the variables—e04wdc is a *gradient-based* optimization method (Snyman, 2005), i.e. it uses information about a function's derivative to find a local minimum. It is in the same class of optimization routines as the *steepest* (or *gradient*) *descent method* and *Newton's method* (Nocedal and Wright, 2006) and, like Newton's method, e04wdc uses the second derivative to take a direct route. The objective and constraint functions are assumed to be smooth, i.e. at least twice-continuously differentiable.

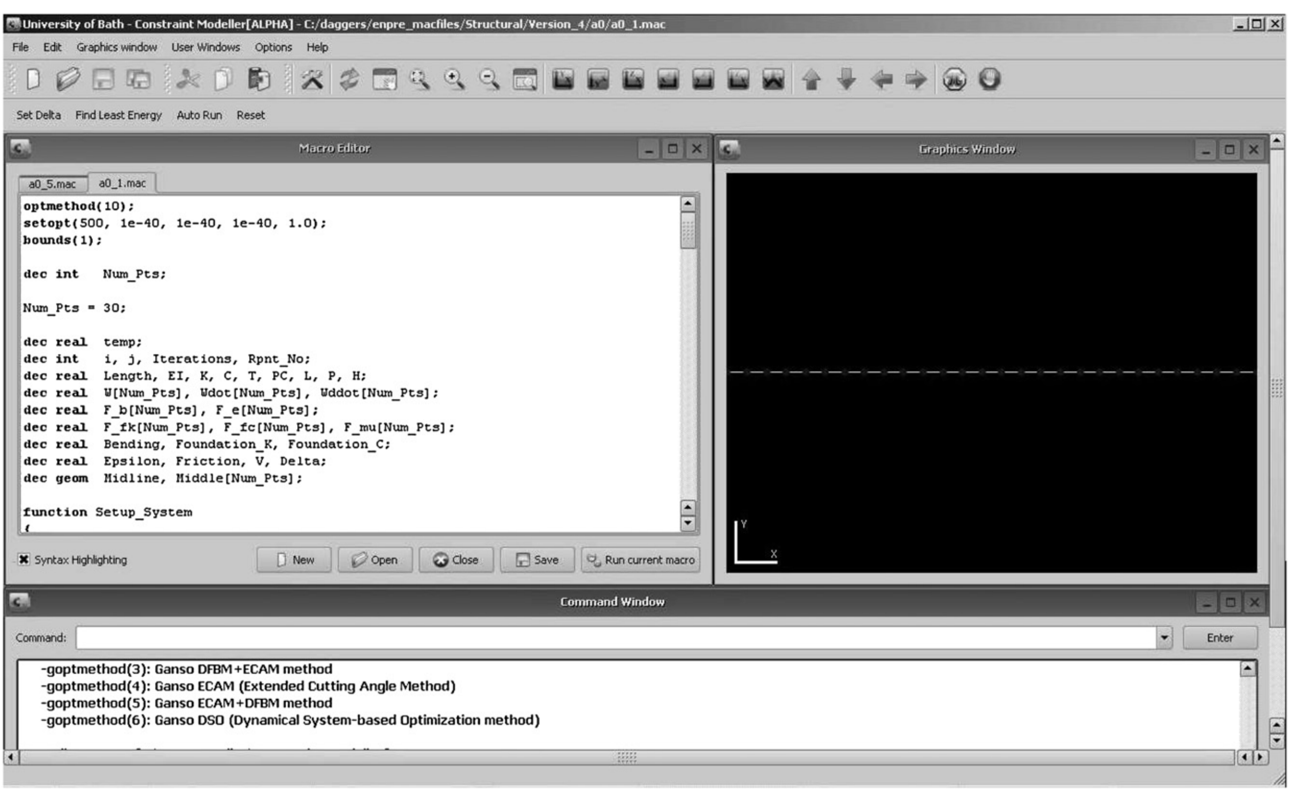

Fig. 7. The constraint-based modeller user interface.

3.2. A constraint-based formulation

To look at a series of solutions, certain values have to be selected a priori. To set-up a constraint-based model, following Section 2.1, take two layers of length *Length*, stiffness *EI* and frictional coefficient μqt, in a matrix of stiffness k. As in Edmunds et al., (submitted for publication), $Length = 100$ mm and a ratio of $\mu qt{:}EI{:}k = 5{:}200{:}1$ is taken. Hence, values for the half-wavelength $L \approx 14.05$ mm and the critical load $P^C = 40$ N are predicted, coming from (5) and (4) respectively. The latter gives a potential lower bound on the load level. Here $\chi = +1$, as the friction is opposing the end-shortening.

Similarly to Edmunds et al., (submitted for publication), the central interface is represented graphically by a number of discrete points, Num_Pts = 50, in two-dimensional space, evenly spaced along the length. With the two end-points fixed in both the horizontal, x' (as x is the arclength, x' is used for the horizontal axis), and vertical, w, directions, the others are allowed to vary in these directions, thus giving 96 degrees-of-freedom. The energy equation (1) is calculated in the function, Energy(), by using an in-built numerical differentiation command and the trapezium rule.

To look for the wave-profile with minimal energy as the end-shortening is increased, the right-hand end of the interface is considered as the "loaded" end of the two layer sample. Positioning the right-hand end at an end-shortening, Δ, and calculating V, via Energy(), the points representing the interface are adjusted using the NAG Library optimization algorithm (NAG, 2005) described in Section 3.1, and an attempt is made to satisfy the following *constraint rules*:

(a) Points have not passed through each other in x'-direction;
(b) The original arc length is maintained by the profile;
(c) The imposed end-shortening (Δ) is equal to the value ($\mathcal{E}$) calculated by Energy;
(d) The energy is minimized.

Additionally there is only one load, P, for a given end-shortening, Δ. This should be found simultaneously with the waveshape. However, Edmunds et al., (submitted for publication) showed that the solutions are highly sensitive and, particularly for small values of Δ, the $V = 0$ solution corresponding to the flat-state tends to dominate (in reality this solution cannot exist as it is within the "jammed" region presented in Section 2.1). Therefore, Edmunds et al. add a second stage to the solution process which tests the load level and it is shown that the local energy minima are better found during this second stage.

From (1), V is linear in the load and thus changing P has little effect on the waveshape if the constraints (a)–(d) are satisfied. However, if the load is too high then it is to be expected that the local minimum energy corresponds to a solution with a larger end-shortening. Similarly, if P is not large enough, then the local energy minimum is achieved with a smaller end-shortening. Hence the minima are unstable, matching the saddle points found in the energy contour plots presented by Hunt et al. (2006), as lower energies are found for the flat state and periodic solution.

Thus to find the solutions of interest, once an output profile has been found, the second stage of the solution process is to release the "loaded", right-hand end of the interface in the x'-direction (giving 97 degrees-of-freedom), and test whether the end-shortening changes (and $\Delta \approx \mathcal{E}$), whilst satisfying (a), (b) and (d). P is therefore adjusted until the solution is stationary.

This two stage solution method can be automated by including a second optimization loop, which varies P such that the correct end-shortening is maintained. Conversely, owing to small iteration steps in the optimization algorithm, a disadvantage of adding the second loop is that the time for a simulation to be completed can be extended approximately tenfold.

4. The full energy formulation

To compare and contrast with the small-deflection solutions illustrated by Edmunds et al., (submitted for publication), attention here is turned to the large-deflection energy formulation, (1). As in that paper, the load paths and the change in the interface profile are followed as the end-shortening increases. Using a constraint-based formulation and solver, the restrictions that faced Hunt et al. (2006) in extending the cubic B-spline model to the full functional are removed.

Edmunds et al., (submitted for publication) showed that by finding the stationary values of the small-deflection energy functional with increasing end-shortening, propagation can be followed without *any* lock-up criterion in the system; however, one must be included to obtain the correct loading. This is done via the incorporation of a stiffening nonlinearity in the foundation through the inclusion of (3) which gives the possibility of restabilization of the axial load. It has been argued by Boon et al. (2007) and Boon (2007) that lock-up is caused by the "cusping" at the centre of the folds; however, it is most likely a combination of foundation and cusping effects, as new folds often start to grow before the current one has reached a point where the singularity alone would have a significant affect.

Starting with $C = 0$ in (3), and thus dealing with a purely linear foundation, solutions are found using the methodology described in Section 3.2, by finding an automatic load level after discovering an approximate value of P manually. As is seen in the subsequent sections, a stiffening nonlinearity needs to be added to the foundation to achieve the desired behaviour from the model and therefore, after Edmunds et al., (submitted for publication), the nonlinear component is set to $C = 0.25$. Owing to the computational time and effort, the automatic optimization loop is not implemented in this second run, as the precision is deemed satisfactory from the initial manual search.

4.1. Results

4.1.1. Linear foundation

To mimic Edmunds et al., (submitted for publication), the end-shortening was increased from $\Delta = 0.5$ to $\Delta = 8.0$ and the solutions found by resolving the constraint-based system using the NAG optimization routine e04wdc (NAG, 2005). Here a larger number of small increments were included in the early stages than previously to improve accuracy. The results of the modelling are shown in Fig. 8.

The first observation that can be made from the P–Δ plot given in Fig. 8(a) is that the load path actually stops at $\Delta \approx 5$. No reasonable solution can be found after this value and the system appears to *lock-up completely*.

Studying the wave-profiles in Fig. 8(b), the loaded end has deformed and even for the final valid solution only the first hump has grown to any significant degree. With a softening linear foundation, the large-deflection formulation easily admits minimum energy solutions with tight, large amplitude, half-waves. The system is softening to a larger degree to create such amplitudes, hence the load–deflection plot for the large-deflection formulation is below that of the small-deflection. In the case presented here, the initial hump has grown to the point that the limbs are almost vertical and with these large deformations problems can appear in the model due to, from (1), the curvature becoming singular in the denominator of bending energy, U_B, and the end-shortening, $\mathcal{E}$, having complex values.

Whilst this might be considered a fault in the set-up of the constraint-based formulation, Boon (2007), when testing multi-layers of differing thicknesses consisting of paper embedded in a foam foundation, remarked upon a similar phenomenon. With a thick surrounding matrix, one that Boon considers to be approximately linear, when (in particular) thick and (occasionally)

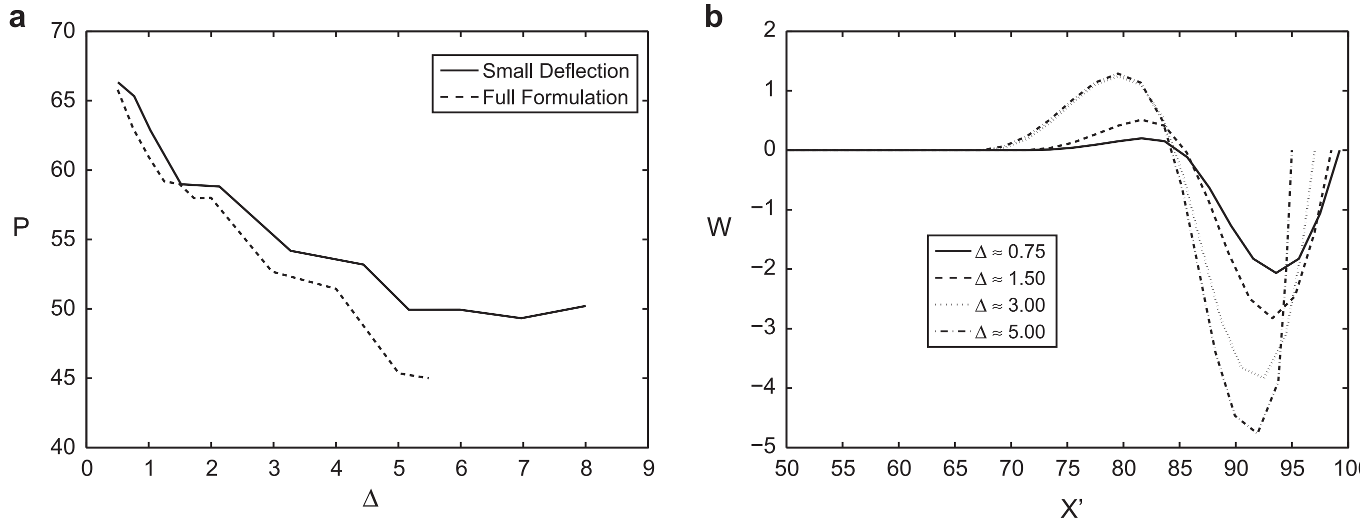

Fig. 8. (a) Load–End-shortening plot and (b) Evolution of the wave-profile as the end-shortening is increased.

thin multilayers buckle at just the loaded end, both are prone to stopping at just two humps, even with "significant" amounts of end-shortening (Boon, 2007) (Fig. 9).

When a nonlinear stiffening element is added to the foundation, such that the load restabilizes, it is to be expected that large amplitudes would be prohibited. Therefore, this regime is now studied.

4.1.2. Nonlinear foundation

As in Edmunds et al., (submitted for publication), the point energy resulting from incorporating a stiffening nonlinearity into the foundation, is calculated in the Energy() function and integrated along the length via the trapezium rule. Thus an approximate value is found for (3), the total energy added to the system in doing this. With C set to 0.25, analysing the full formulation with this addition for $\Delta = 0.5–8.0$, Fig. 10 gives the resulting $P–\Delta$ plot. As with the small-deflection results (Edmunds et al., (submitted for publication)), there is a definite destabilizing then restabilizing of the load path, although the increments in the end-shortening are not small enough to make it completely clear that each decrease in stiffness coincides with a new hump forming.

Of more interest are the wave-profiles presented in Fig. 11. Two things are immediately apparent from looking at these profiles: firstly the amplitudes of the wave are smaller than in Fig. 8(b), the system no longer "locks up" and more end-shortening can be applied to the layers to give multiple humps; secondly, in the initial stages, both ends of the sample—the loaded and the reactive—deform at about the same time. However, the waveshape is slightly different for each end and here the loaded end continues to evolve for much of the loading, only in the latter stages does the reactive end start to change to any extent.

Again, even though this might be considered an artefact of the modelling process, such behaviour has been in seen in experiments (Boon, 2007; Boon et al. (in press)). Fig. 12(a) and (b) were taken from an experiment conducted during the set that appeared in Edmunds et al. (2006). Here the foundation had a high transverse load such that the nonlinear stiffening was more noteworthy, and showed exactly the same features as those resulting from the model (Fig. 11). Note the tight concentric waves at the loaded end and the more open sinusoidal waves at the reactive end. The difference in shape of the waves at each end, which one propagates as the dominant buckle pattern and how this influences the load path, is discussed in greater detail by Boon et al. (in press). In contrast, the focus is now turned to a very interesting possible extension of the concentric parallel folding formulation.

5. Changing the behaviour to kink banding

Finally a study on the related geological buckling phenomenon of kink banding, also known as box folding, is now presented. These preliminary findings, using constraint-based modelling, show the possible admittance of box folds as a solution appearing directly

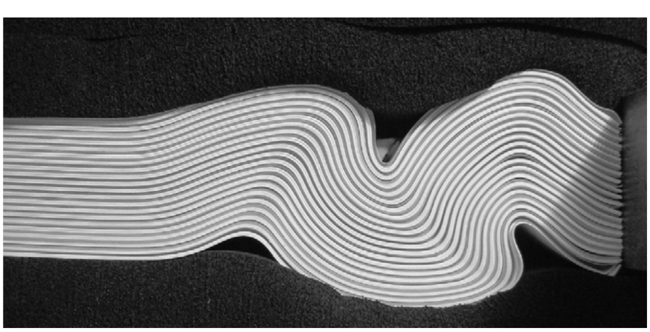

Fig. 9. A "thick" multilayer that has completely locked up at two humps. (After Boon, 2007).

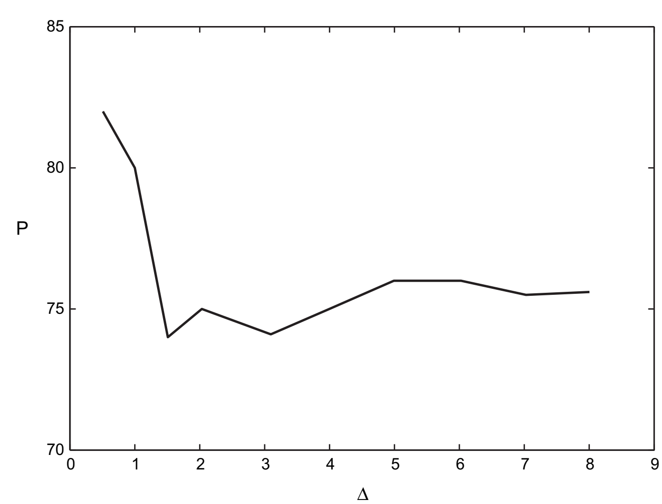

Fig. 10. $P–\Delta$ plot with a nonlinear foundation.

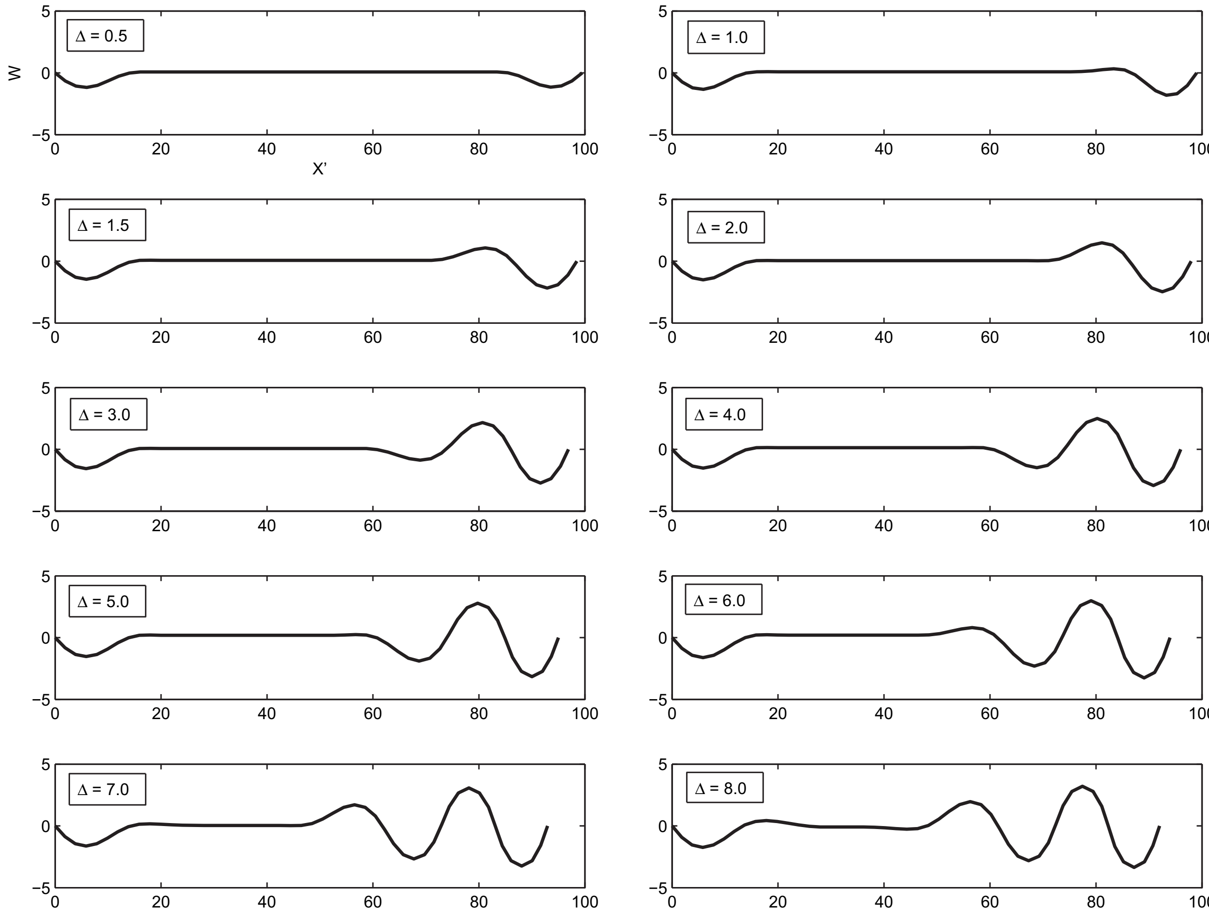

Fig. 11. The wave-profile as the end-shortening is increased.

from the concentric parallel folding formulation. Such results need to be studied in more depth in the future and further research will be conducted to clarify the emergence of the waveshapes.

5.1. Kink band energy formulation

Like concentric folding, kink banding is often found in the deformation of geological strata (Price and Cosgrove, 1990) and is a potential failure mode for a layered material held together by an external pressure, subjected to layer-parallel compression. Again occurring under huge overburden pressures, the difference between concentric folding and kink banding regimes is that the foundation is much stiffer in the latter than the former. By considering the large transverse pressure and interlayer slippage, as with concentric parallel folding, a model has been formulated in terms of elastic bending and friction (Hunt et al., 2000b) and extended in several articles (Hunt et al., 2001; Wadee et al., 2004). A brief outline of the formulation is now given.

As before, voids incur large energy penalties and therefore the resulting wave-profile negates these in nature. As shown experimentally in Fig. 2, using layers of paper, and schematically in Fig. 13, the layers are unable to deform into the surrounding matrix and to penalize voids, kink bands are characterized by having straight limbs and sharp corners (Hunt et al., 2000b). Hence within the multilayer, each layer takes the same waveshape as its neighbours.

To this end, the model is set up by assuming that there is a stack of n layers of thickness t, width a_1 and length a_2 which is loaded axially and confined transversely by distributed forces of total

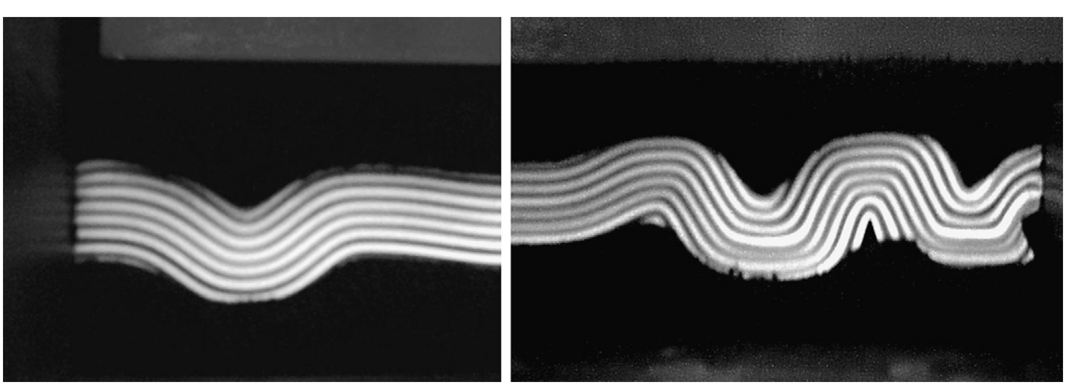

Fig. 12. (a) Left-hand (reactive) end and (b) Right-hand (loaded) end of the sample.

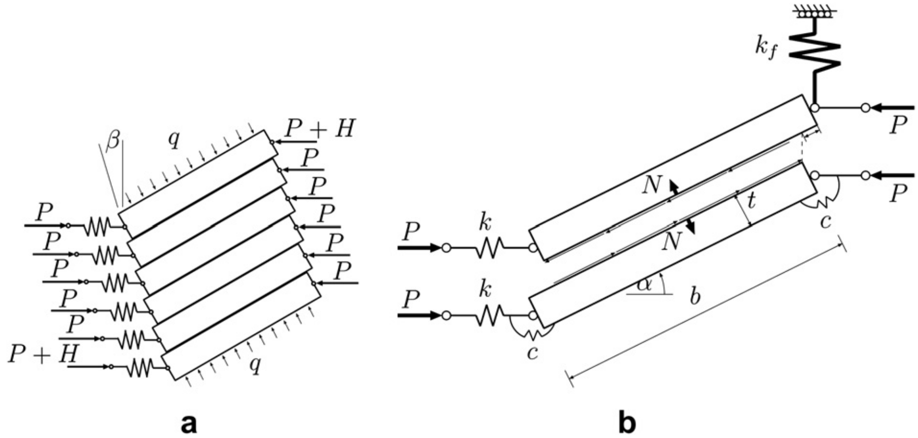

Fig. 13. (a) Stack of blocks at orientation angle β with layer-parallel stiffness k. (b) Representative two-layer section, showing single layer contributions to the bending stiffness c (lower layer) and the "foundation" stiffness k_f (upper layer). (After Wadee and Edmunds, 2005).

magnitude nP and Q respectively. Hence, the overburden pressure is defined as $q = Q/a_2$ and the distributed layer-parallel load on each layer is given by $p = P/t$. As with the concentric parallel folding model, the friction force between the layers is modelled by a Coulomb friction law with a coefficient μ.

Additionally from Fig. 13, the following variables are included:

- The kink band orientation angle β;
- The angle of rotation α;
- The layer bending stiffness, modelled as rotational spring of stiffness c;
- The stiffness of the surrounding layers (analogous to foundation stiffness) k_f;
- The kink band width b.

To calculate the total potential energy it is necessary to consider:

(i) The sum of strain energy from compressing layer-parallel springs of stiffness k;
(ii) Rotating the springs of stiffness c to simulate bending energy (note that this c is not the same as the nonlinear foundation stiffness C in the concentric parallel folding model);
(iii) Evaluating the energy required to overcome the frictional force as the layers slide over each other;
(iv) Compressing the foundation springs of stiffness k_f;
(v) The work done by the external loads axially and transversely.

For kink band i, the potential energy, V_i, nondimensionalized with respect to $k_i t^2$, is given by:

$$V_i = \underbrace{\frac{1}{2}\delta_i^2}_{\text{(i)}} + \underbrace{c_i\alpha_i^2}_{\text{(ii)}} + \underbrace{\mu q_i b_i \int_0^{\alpha_i}\left[\frac{(1-\cos(\alpha-\beta_i))\cos(\alpha-\beta_i)}{(1-\cos\beta_i)(1-\mu\tan\alpha)}\right]\mathrm{d}\alpha}_{\text{(iii)}}$$
$$+\underbrace{\frac{1}{2}k_{f_i}b_i^2\sin^2\alpha_i}_{\text{(iv)}} - \underbrace{p\delta_i - (p-q_i)b_i(1-\cos\alpha_i)}_{\text{(v)}}, \qquad (6)$$

where each expression in (6) follows respectively (i)–(v). Full details of the formulation and derivation of each element in the total potential energy can be found in Wadee et al. (2004). Stationary solutions of (6) with respect to α_i, b_i and end-shortening δ_i lead to load–deflection paths and values for α_i and β_i, that can be compared with experimental results.

By comparing the model and experiments using layers of paper, the outer layers surrounded by a steel rig used as a foundation, there is very good correlation for not only the initial instability, rotation and orientation angles (α and β respectively in Fig. 13)

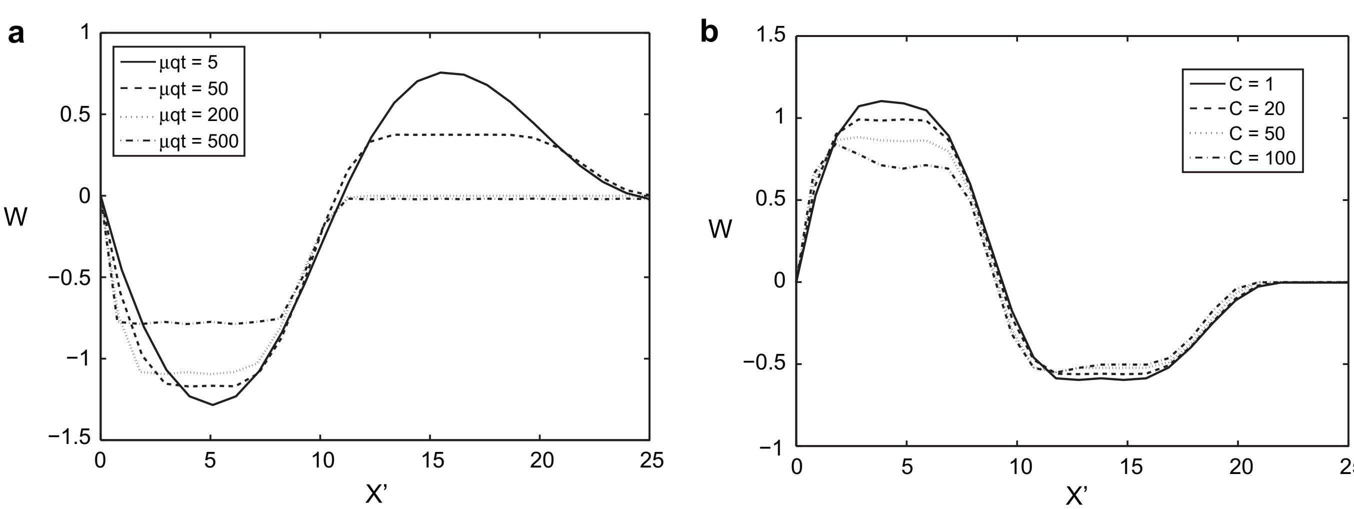

Fig. 14. Changing from a concentric fold to a box fold? Central interface wave-profiles with (a) Increasing overburden pressure, (b) Increasing nonlinear stiffening. (Note: the deformation has started at the *reactive* end, in accord with Boon et al. (in press) who agree that both evolutions are possible.).

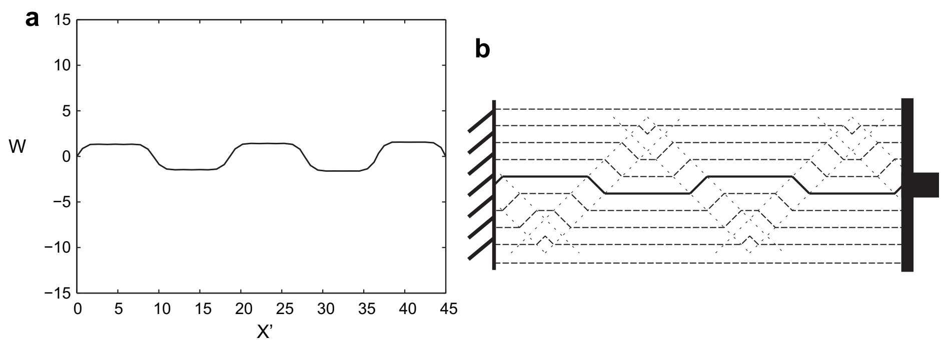

Fig. 15. (a) "Box fold"-like wave profile of the central interface when $\Delta = 5$, $\mu qt = 200$, (b) Schematic showing the central interface extended.

(Wadee et al., 2004), but also for subsequent ones after propagation (Wadee and Edmunds, 2005).

It should be stated that the formulation that leads to (6) assumes a priori the waveshape, leading to the parameters—angles β and α, plus band width b—that allow the shape evolution to be tracked throughout each instability. The results that follow do not supersede the kink band model described above, there is no way thus far to predict the instabilities nor the angles in the current formulation for example; however, in imposing the constraints, a wave with a kink band-like fold profile can result directly from the concentric parallel folding model. Thus the idea that the phenomena of kink bands and concentric folds are related is reinforced, a "phenomenological trigger" being shown to change between them.

5.2. Constraint-based formulation

The wish here is to explore the differences between the two scenarios of concentric folding and kink banding, thus giving some insight into the relationship between the two fold-types. No attempt is made to directly create a constraint-based model for (6), rather, by altering the relevant variables in the constraint-based concentric parallel folding formulation, it is shown that it is possible to get both profiles.

From kink banding experiments (Wadee et al., 2004; Wadee and Edmunds, 2005), two points become apparent when compared to concentric folding. For kink banding: first the foundation stiffness is much higher in relation to the layer stiffness and second the overburden pressure is significantly larger. In fact, for the former, from Wadee and Edmunds (2005), the ratio of foundation stiffness and layer stiffness is tending towards unity $EI{:}k \approx 6{:}1$. From the same article, the overburden required for the initiation of kink bands is at least 10 times higher than that used in the equivalent concentric folding experiments shown by Edmunds et al. (2006).

However, with the external layers comprising the multilayer giving the basal slip zones, this might be thought of as an "effective" stiffness for the foundation coming from the high overburden. What is clearer is that the softening (linear) part of the foundation is quickly dominated by the stiffening nonlinear part as the multilayer tries to move into an unyielding medium.

Therefore, as an initial investigation, the constraint-based model for concentric parallel folding under small deflections as described by Edmunds et al., (submitted for publication) is used, with the ratio of the stiffnesses for the layers and linearity in the foundation as given in Section 3.2, $EI{:}k = 200$. As mentioned above, it is assumed that the overburden changes the behaviour rather than altering the ratio $EI{:}k$. As the nonlinear component of the foundation stiffness is more dominant than in concentric folding this is reflected in the energy formulation and thence, with no measured value available, a ratio of $k{:}C = 1$ is chosen initially. This larger value of C is reasonable as it has the effect of giving a low amplitude wave with longer wavelengths—the humps are unable to close significantly and it is much easier to form the next in the sequence than move further into the matrix—something that is noticeable in kink banding at the central interface.

The effect of increasing the overburden on the waveshape is less obvious, but it is expected to force the rounded concentric waves to "square off" and flatten. To test this hypothesis, values for the end-shortening Δ and load P are fixed (as no attempt is made at this point to establish the loading paths, these values are not so important) and μqt is incrementally increased. To find the least energy wave profile the *constraint rules* given in Section 3.2 are minimized, in particular the condition $\Delta = \mathcal{E}$ is imposed.

To see the change in preferred shape more precisely the interfacial length was halved (i.e. Length = 50 mm), whilst the number of points representing this, Num_Pts, was kept at 50 as previously.

5.2.1. Results

To follow the evolution of the preferred waveshape, the end-shortening was originally set at $\Delta = 0.5$ and the variable incorporating the overburden pressure μqt was increased from 5 to 500. The results from this are shown in Fig. 14(a).

Satisfyingly, there is a definite transition in the preferred waveshape from a very curved one, that is "concentric fold"-like in geometry, to a much more flat one with straight limbs, that shows a strong resemblance to centre of a *box fold*. Whilst the higher values might be considered outside the feasible range seen experimentally, this change begins to occur at $\mu qt = 50$, i.e. 10 times higher than that required for concentric folding. Keeping the overburden effect at 50 and putting C at a larger value, little occurs until $C \approx 20$ where the "box"-shape is even more marked (Fig. 14(b)). Beyond $C \approx 50$ the profile begins to take a waveshape that is not found in experiments and, as a result, is not discussed further here.

(Note: it is very important to state here that apart from the initial solution, these solutions cannot currently be obtained directly. Having found the least energy wave for $\mu qt = 5$ and $C = 1$, the others can be found by changing μqt or C and optimizing from that profile. Hence each profile in Fig. 14 is found having obtained the previous one. It is hoped that this can be addressed in the future).

By putting $\Delta = 5.0$, $C = 1$ and $\mu qt = 200$, the box-fold waveshapes at the central interface are even more apparent (Fig. 15(a)). As illustrated in the schematic of Fig. 15(b), extending the geometry in both directions a sequence of kink bands is clearly observable.

6. Conclusions

This paper has taken a recently established elastic, frictional model for two layer concentric parallel folding and compared its predictions with experiments. More layers will be added in the future by combining the multilayer formulation presented by Edmunds et al. (2006) with the geometric restrictions studied by

Boon et al. (2007). By representing the central interface as a series of points, a constraint-based formulation is created. Formulating a set of *constraint rules* that must be satisfied and, starting from an initially flat state, the loaded end of the interface is disturbed with a given end-shortening. Using a NAG Library optimization routine (NAG, 2005) to ensure that all of the constraints hold true, and then relaxing several of these, load levels and the corresponding least energy solutions for the end-shortening can be found with ease.

Incrementally increasing the end-shortening and repeating, unlike the B-spline model given in Hunt et al. (2006) which is computationally complicated, the evolution of the central interface is followed for many humps and the resulting load paths and wave-profiles successfully match the experimental data of Edmunds et al. (2006) and Boon et al. (in press).

Unlike the small-deflection model, where the sequential propagation is clearly seen without an included *lock-up* criterion or nonlinearity in the foundation, for the full formulation with a purely linear foundation, no solutions can be found beyond the second hump. The system reaches a point of lock-up, agreeing with experimental evidence that seems to suggest that this is a likely outcome (Boon, 2007; Boon et al. (in press)). However, like the small-deflection scenario, inclusion of a linear foundation does not produce the destabilization and restabilization of the load-deflection paths as observed in experiments.

Adding a small hardening nonlinear stiffness to the foundation, the P–Δ plots are more realistic and, as is again indicated from the profiles resulting from experiments, this overcomes the lock-up. Thus the simulations match the process of forming concentric parallel folds closely, even potentially showing the buckling that can form at both ends of the sample in this regime. More experiments are needed, but details about this behaviour will be given in a forthcoming paper (Boon et al. in press).

Finally, a scoping investigation has been presented, showing that it is possible to produce kink band-like structures from the concentric folding formulation. Using the small-deflection model, increasing the nonlinearity in the foundation and the magnitude of the overburden, the central interface begins to take on a box fold wave-profile and thus encompasses the transition between several different folding-types seen in nature. This study is in the very early stages, certainly the overburden values that make the shape very prominent are beyond what is achieved experimentally and whilst altering the nonlinear part of the foundation seems to add to this effect, the correct magnitude is speculative. Additionally the box folds cannot currently be found as an immediate solution, it is necessary to evolve towards them from another solution.

Therefore there is a definite need to investigate kink banding further, starting with an attempt to get a measure of the magnitude of the nonlinear variable C from experiments. Using the constraint-based model, is it possible to get the correct output shapes from a flat state? If it is possible, what affects this? The intention is to explore these factors in the near future, such that it is then possible to successfully follow the load-deflection plots in a similar way to the concentric parallel folding model presented here. As part of this, it may be required to use the large-deflection energy functional.

Acknowledgements

The work reported in this paper has been undertaken as part of the EPSRC Innovative Design Manufacturing Research Centre at the University of Bath (grant reference GR/R67507/0). The authors gratefully acknowledge this support and express their thanks for the advice and support of all concerned.

References

Biot, M.A., 1961. Theory of folding of stratified viscoelastic media and its implication in tectonics and orogenesis. Bull. Geol. Soc. Amer. 72, 1595–1620.
Biot, M.A., 1963. Theory of stability of multilayer continua in finite anisotropic elasticity. J. Franklin Inst. 276, 128–153.
Biot, M.A., 1964. Theory of internal buckling of a confined mutilayered structure. Bull. Geol. Soc. Amer. 75, 563–568.
Biot, M.A., 1965. Mechanics of Incremental Deformations. Wiley, New York.
Blay, P., Cosgrove, J.W., Summers, J.M., 1977. An experimental investigation of the development of structures in multilayers under the influence of gravity. J. Geol. Soc. London 133, 329–342.
Boon, J.A., 2007. Level set methods for multilayer geological folding. Ph.D. thesis, University of Bath, UK.
Boon, J.A., Budd, C.J., Hunt, G.W., 2007. Level set methods for the displacement of layered materials. Proc. R. Soc. Lond. A 463, 1447–1466.
Boon, J.A., Budd, C.J., Edmunds, R., Hunt, G.W. Level set modelling for the parallel folding of layered structures: Comparisons with experiments. J. Mech. Phys. Solids, in press.
Budd, C.J., Hunt, G.W., Kuske, R., 2001. Asymptotics of cellular buckling close to the Maxwell load. Proc. R. Soc. Lond. A 457, 2935–2964.
Budd, C.J., Edmunds, R., Hunt, G.W., 2003. A nonlinear model for parallel folding with friction. Proc. R. Soc. Lond. A 459, 2097–2119.
Cobbold, P.R., 1975. Fold propagation in single embedded layers. Tectonophysics 27, 333–351.
Donath, F.A., Parker, R.B., 1964. Folds and folding. Bull. Geol. Soc. Amer. 75, 45–62.
Edmunds, R., Hunt, G.W., Wadee, M.A., 2006. Parallel folding in multilayered structures. J. Mech. Phys. Solids 2, 384–400.
Edmunds, R., Hicks, B.J., Mullineux, G. Using constraint-satisfaction as a means for modelling parallel folding evolution. IMA J Appl. Math, submitted for publication.
Edmunds, R., Wadee, M.A., 2005. On kink banding in individual PPTA fibres. Compos. Sci. Tech. 7–8, 1284–1298.
Hicks, B.J., Medland, A.J., Mullineux, G., 2001. A constraint-based approach to the modelling and analysis of packaging machinery. Packag. Technol. Sci. 14, 209–225.
Hicks, B.J., Medland, A.J., Mullineux, G., 2006. The representation and handling of constraints for the design, analysis, optimization of high speed machinery. AIEDAM 20, 313–328.
Hobbs, B.E., Means, W.D., Williams, P.F., 1976. An Outline of Structural Geology. Wiley, Brisbane.
Hunt, G.W., 2006. Buckling in space and time. Nonlinear Dyn. 43, 29–46.
Hunt, G.W., Wadee, M.K., Shiacolas, N., 1993. Localized elasticae for the strut on the linear foundation. ASME J. Appl. Mech. 60, 1033–1038.
Hunt, G.W., Peletier, M.A., Champneys, A.R., Woods, P.D., Wadee, M.A., Budd, C.J., Lord, G.J., 2000a. Cellular buckling in long structures. Nonlinear Dynam 21 (1), 3–29.
Hunt, G.W., Peletier, M.A., Wadee, M.A., 2000b. The Maxwell stability criterion in pseudo-energy models of kink banding. J. Struct. Geol. 22 (5), 669–681.
Hunt, G.W., Wadee, M.A., Peletier, M.A., 2001. Friction models of kink banding in compressed layered structures. In: Mühlhaus, H.B., Dyskin, A.V., Pasternak, E. (Eds.), Proceedings of the 5th International Workshop on Bifurcation and Localization in Geomechanics (IWBL99). Swets & Zeitlinger, Lisse, pp. 249–256.
Hunt, G.W., Edmunds, R., Budd, C.J., Cosgrove, J.W., 2006. Serial parallel folding with friction: a primative model using cubic B-splines. J. Strut. Geol. 28, 444–455.
Hunt, G.W., Wadee, M.A., 1998. Localization and mode interaction in sandwich structures. Proc. R. Soc. Lond. A 454, 1197–1216.
Johnson, A.M., 1977. Styles of Folding. Elsevier, Amsterdam.
Matthews, J., Singh, B., Mullineux, G., Medland, A.J., 2006. Constraint-based approach to investigate the process flexibility of food processing equipment. Comput. Ind. Eng. 54 (4), 809–820.
Mitchell, R.H., Medland, A.J., Salo, A.I.T., 2007. A design methodology to create constraint-based human movement patterns for ergonomic analysis. J. Eng. Des. 18 (4), 293–310.
Mullineux, G., 2001. Constraint resolution using optimization techniques. Comput. Graph. 25, 483–492.
Mullineux, G., Hicks, B.J., Medland, A.J., 2005. Constraint-aided product design. Acta Polytechnica 45 (3), 31–36.
Mullineux, G., Matthews, J., 2010. Constraint-based simulation of carton folding operations. Comput. Aided Des 42 (3), 257–265.
NAG, 2005. NAG C Library Manual—Mark 8. Tech. Rep. The Numerical Algorithms Group Limited.
Nocedal, J., Wright, S.J., 2006. Numerical Optimization, second ed. Springer, New York.
Peletier, M.A., 2001. Sequential buckling: a variational analysis. SIAM J. Math. Anal. 32 (5), 1142–1168.
Price, N.J., 1970. Laws of rock behaviour in the Earth's crust. In: Sommerton, W.H. (Ed.), Rock Mechanics—Theory and Practice. Proceeding of 11th Symposium of Rock Mechanics. A.I.M.M., pp. 3–23.
Price, N.J., 1975. Rates of deformation. J. Geol. Soc. Lond. 131, 553–575.
Price, N.J., Cosgrove, J.W., 1990. Analysis of Geological Structures. Cambridge University Press, Cambridge.
Ramberg, H., 1961. Contact strain and folding instability of a multilayered body under compression. Geol. Rundsch. 51, 405–439.
Ramberg, H., Strömgård, K.E., 1971. Experimental tests of modern buckling theory applied on multilayered media. Tectonophysics 11, 461–472.

Singh, B., Matthews, J., Mullineux, G., Medland, A.J., 2010. Design catalogues for mechanism selection. Proceeding of 10th International Design Conference. Design 2008, pp. 673–680.
de Sitter, L.U., 1964. Structural Geology. McGraw–Hill, New York.
Snyman, J.A., 2005. Practical Mathematical Optimization: An Introduction to Basic Optimization Theory and Classical and New Gradient-Based Algorithms. Springer, Boston.
Thompson, J.M.T., Hunt, G.W., 1973. A General Theory of Elastic Stability. Wiley, London.
Wadee, M.A., Edmunds, R., 2005. Kink band propagation in layered structures. J. Mech. Phys. Solids 53 (9), 2017–2035.
Wadee, M.A., Hunt, G.W., Peletier, M.A., 2004. Kink band instability in layered structures. J. Mech. Phys. Solids 52 (5), 1071–1091.